

RESEARCH ARTICLE

Mitoflash biogenesis and its role in the autoregulation of mitochondrial proton electrochemical potential

Gaomin Feng, Beibei Liu, Jinghang Li, Tianlei Cheng¹, Zhanglong Huang, Xianhua Wang², and Heping (Peace) Cheng¹

Respiring mitochondria undergo an intermittent electrical and chemical excitation called mitochondrial flash (mitoflash), which transiently uncouples mitochondrial respiration from ATP production. How a mitoflash is generated and what specific role it plays in bioenergetics remain incompletely understood. Here, we investigate mitoflash biogenesis in isolated cardiac mitochondria by varying the respiratory states and substrate supply and by dissecting the involvement of different electron transfer chain (ETC) complexes. We find that robust mitoflash activity occurs once mitochondria are electrochemically charged by state II/IV respiration (i.e., no ATP synthesis at Complex V), regardless of the substrate entry site (Complex I, Complex II, or Complex IV). Inhibiting forward electron transfer abolishes, while blocking reverse electron transfer generally augments, mitoflash production. Switching from state II/IV to state III respiration, to allow for ATP synthesis at Complex V, markedly diminishes mitoflash activity. Intriguingly, when mitochondria are electrochemically charged by the ATPase activity of Complex V, mitoflashes are generated independently of ETC activity. These findings suggest that mitoflash biogenesis is mechanistically linked to the build up of mitochondrial electrochemical potential rather than ETC activity alone, and may functionally counteract overcharging of the mitochondria and hence serve as an autoregulator of mitochondrial proton electrochemical potential.

Introduction

Being the so-called cellular powerhouse, mitochondria synthesize the energy currency ATP through oxidative phosphorylation mediated by the inner membrane-bound electron transfer chain (ETC) and ATP synthase (Complex V; Mitchell, 1966). The ETC consists of Complexes I, II, III, and IV, which couple the free energy released from electron transfer to pumping matrix protons into the intermembrane space, building up a pH gradient across the inner membrane and contributing to the mitochondrial membrane potential ($\Delta\Psi_m$). Their combination constitutes the proton electrochemical potential ($\Delta\mu_{H^+}$), which drives ATP synthase (Complex V)-mediated ATP synthesis through downhill proton influx. During electron transfer, a small fraction of electrons can also be diverted from the ETC by molecular oxygen to form superoxide, the primal reactive oxygen species (ROS). Thus, an emerging view is that mitochondria also play an essential role in cellular ROS signaling and redox homeostasis (Mailloux, 2015; Shadel and Horvath, 2015).

We and others have previously shown that respiring mitochondria undergo dynamic changes in the form of

“mitochondrial flashes (mitoflashes),” which comprise multiplex signals, including bursting superoxide production, transient matrix alkalization, oxidative redox shift, oxidation of NADH and flavin adenine dinucleotide (FADH₂), and dissipation of the $\Delta\Psi_m$ (Wang et al., 2008, 2016; Pouvreau, 2010; Wei-LaPierre et al., 2013; Breckwoldt et al., 2014). From the viewpoint of bioenergetics, a mitoflash represents transient uncoupling of mitochondrial respiration from ATP production (Feng et al., 2017; Wang et al., 2017). The mitoflash is ubiquitous in eukaryotic species ranging from *Caenorhabditis elegans* to zebrafish and to rodents and humans (Wang et al., 2008; Shen et al., 2014; Zhang et al., 2015). Its frequency can be regulated over orders of magnitude by varying the substrate supply (Pouvreau, 2010; Fang et al., 2011; Wei et al., 2011; Gong et al., 2015; Wang et al., 2017) as well as by changes in mitochondrial ETC supercomplex dynamics (Jian et al., 2017). Moreover, prominent mitochondrial signals, including basal ROS (Hou et al., 2013; Zhang et al., 2014), matrix Ca²⁺ (Hou et al., 2013; Jian et al., 2014), and matrix protons in the nanodomains of the inner mitochondrial membrane (Wang et al.,

State Key Laboratory of Membrane Biology, Beijing Key Laboratory of Cardiometabolic Molecular Medicine, Institute of Molecular Medicine, Peking-Tsinghua Center for Life Sciences, Peking University, Beijing, China.

Correspondence to Xianhua Wang: xianhua@pku.edu.cn.

© 2019 Feng et al. This article is distributed under the terms of an Attribution-Noncommercial-Share Alike-No Mirror Sites license for the first six months after the publication date (see <http://www.rupress.org/terms/>). After six months it is available under a Creative Commons License (Attribution-Noncommercial-Share Alike 4.0 International license, as described at <https://creativecommons.org/licenses/by-nc-sa/4.0/>).

2016), constitute potent mitoflash regulators. Surprisingly, in intact cells, mitoflash activity is repressed by all ETC inhibitors examined and is even sensitive to the inhibition of ATP synthase activity (Wang et al., 2008; Zhang et al., 2013), suggesting that mitoflash biogenesis might require intact oxidative phosphorylation. All these findings have established a close linkage between mitoflash production and mitochondrial energy metabolism. Indeed, we have recently shown that mitoflashes inhibit ATP synthesis in isolated mitochondria and regulate the setpoint of ATP homeostasis in cardiomyocytes (Wang et al., 2017). Nevertheless, how exactly the different ETC complexes are involved in mitoflash biogenesis and what specific role the mitoflash plays in mitochondrial bioenergetics remain open questions.

In the present study, we systematically investigated mitoflash biogenesis in isolated cardiac mitochondria supported by different substrates under different respiratory states. The questions we aimed to address included (1) whether both ETC activity and oxidative phosphorylation are required for mitoflash biogenesis, (2) the simplest condition required for mitoflash biogenesis, and (3) how the mitoflash responds to alterations in mitochondrial bioenergetics. By answering these mechanistic questions, we strove to infer the cell and organelle logic of mitoflash biogenesis in relation to mitochondrial bioenergetics and ROS signaling.

Materials and methods

Animal care

All animal experiments were performed according to the rules of the American Association for the Accreditation of Laboratory Animal Care International and the Guide for the Care and Use of Laboratory Animals published by the U.S. National Institutes of Health (NIH Publication No. 85–23, revised 1996). All procedures were approved by the Animal Care Committee of Peking University accredited by American Association for the Accreditation of Laboratory Animal Care International (IMM-ChengHP14).

Reagents

Rotenone, malonate, antimycin A, NaN_3 , oligomycin, glutamate, malate, succinate, ascorbate, N,N,N',N'-tetramethyl-p-phenylenediamine (TMPD), ADP, ATP-Mg, adenylyl-imidodiphosphate (AMP-PNP), pericidin A, and myxothiazol were from Sigma-Aldrich. Atpenin A5 was from Santa Cruz Biotechnology. Potassium cyanide (KCN) was from the Department of Chemistry, Peking University. Tetramethylrhodamine methyl ester (TMRM) was from Molecular Probes (Thermo Fisher Scientific). Other reagents were obtained commercially at the highest grade available.

Isolation of cardiac mitochondria

Cardiac mitochondria were isolated from mitochondria-targeted (mt)-circularly permuted (cp) YFP transgenic mice as previously reported with some modifications (Wang et al., 2008; Zhang et al., 2013). Briefly, mouse hearts were washed with ice-cold isolation buffer (300 mM sucrose, 5 mM HEPES, 1 mM EGTA, and 0.5 mg/ml BSA, pH 7.2), minced, and homogenized. The homogenate was centrifuged at 4°C for 10 min at 600 *g*. The

supernatant was collected and further centrifuged at 4°C for 10 min at 6,000 *g*. The pellet was resuspended in isolation buffer and centrifuged onto polylysine-coated coverslips at 4°C for 10 min at 4,000 *g*. For imaging, mitochondria were placed in experimental solution (125 mM KCl, 2 mM K_2HPO_4 , 5 mM MgCl_2 , 10 mM HEPES, and 1 mg/ml BSA, pH 7.4) with the addition of different substrates. Mitochondria were stored on ice and used for experiments within 4 h of preparation.

Confocal imaging

An inverted confocal microscope (Zeiss Laser Scanning Confocal Microscope [LSM] 710) with a 63 \times , 1.4 numerical aperture oil-immersion objective was used for imaging. For TMRM measurement, 50 nM TMRM was loaded into mitochondria at room temperature. To obtain cpYFP and TMRM signals simultaneously, images were captured by exciting sequentially at 488, 405, and 543 nm and collecting the emission at 505–530, 505–530, and >560 nm, respectively.

For mitoflash detection, usually 100 frames of 512 \times 512 (xy) pixels were collected at 1 s/frame in bidirectional scanning mode. The size of the imaging region was 44.9 \times 44.9 μm . All of the experiments were performed at room temperature (22–26°C) unless specified otherwise.

Image processing and mitoflash analysis

The time-lapse LSM files generated from the Zeiss LSM 710 were analyzed using custom-developed programs written in interactive data language (IDL Research Systems). Mitoflashes were identified with the help of Flashsniper (Li et al., 2012), and their morphological and kinetic properties, including amplitude and duration, were measured automatically.

Statistics

Data are expressed as means \pm SEM. Student's *t* test was applied to determine statistical significance. One-way ANOVA with post hoc Tukey was used to compare the differences among three or more groups. The χ^2 test was applied to determine the significance of correlation analysis. $P < 0.05$ was considered statistically significant.

Online supplemental material

Fig. S1 shows establishment of the mitochondrial membrane potential by adding different respiratory substrates in state II/IV respiration. Fig. S2 shows the unitary properties of mitoflashes generated under different experimental conditions. Fig. S3 shows the effects of inhibitors on the basal level of mitochondrial TMRM fluorescence.

Four videos show mitoflash occurrence supported by Complex I substrates (Video 1), Complex II substrate (Video 2), Complex IV substrates (Video 3) in state II/IV respiration, and ATP hydrolase (ATPase)-mediated ATP hydrolysis (Video 4).

Results

Mitoflashes supported by Complex I or Complex II substrates

To investigate the involvement of different ETC complexes in mitoflash biogenesis, we used the isolated cardiac mitochondria

system for precise control of metabolic substrates and respiratory states as well as manipulation with ETC inhibitors. Mitochondria were isolated from mt-cpYFP transgenic mouse hearts (Wang et al., 2008). In the first set of experiments, various respiratory substrates without ADP were added to ensure the mitochondria were under state II/IV respiration, i.e., the mitochondrial ETC operated in the absence of ATP synthesis (Fig. 1, A and D; Fig. 2 A; and Fig. S1 A). In the presence of glutamate and malate, electrons from NADH entering the ETC at Complex I are transferred through the entire ETC network consisting of Complexes I, III, and IV, each pumping matrix protons outward into the intermembrane space (Fig. 1 A). Alternatively, succinate was used as the respiratory substrate for electrons to enter the ETC at Complex II and to pass through Complexes II, III, and IV (Fig. 1 D).

As expected, $\Delta\Psi_m$ measured with TMRM was established shortly after adding either Complex I or Complex II substrates while basal cpYFP fluorescence was slightly increased; the latter may reflect matrix alkalization due to proton efflux (Fig. S1 B). Confocal time-lapse imaging visualized the occurrence of robust mitoflashes reported with cpYFP after stabilization of experimental conditions (Fig. 1, A, B, D and E; and Videos 1 and 2). These ETC substrate-supported mitoflashes exhibited unitary characteristics similar to those reported in intact cells, with an average amplitude of ~ 0.6 -fold in the peak fluorescence of cpYFP over the baseline ($\Delta F/F_0$) and an average full duration at half maximum of ~ 4 s (Fig. 1, A and D; and Fig. S2). Next, we applied a panel of inhibitors targeting the ETC at different sites: rotenone for Complex I, malonate or atpenin A5 for Complex II, antimycin A for Complex III, and KCN or NaN_3 for Complex IV (Fig. 1, A and D). We found that all these inhibitors, except for the Complex II inhibitors, abolished the Complex I substrate-supported mitoflashes (Fig. 1 B), indicating that all ETC complexes except for Complex II participate in mitoflash production when the ETC is activated at Complex I. The slight inhibition of mitoflashes by the Complex II inhibitor atpenin A5 (Fig. 1 B) is consistent with its effect of repressing Complex I activity (Miyadera et al., 2003). By contrast, the mitoflashes supported by Complex II substrate were totally repressed by the Complex II, III, and IV inhibitors, while the Complex I inhibitor rotenone had little effect (Fig. 1 E), indicating that Complex I is dispensable for the genesis of mitoflashes under this experimental condition. As indicated in Fig. 1, A and D, these results imply that electron transfer up to the end of the respiratory chain is necessary for mitoflash production, and electrons from Complex I substrates skip Complex II; hence, inhibition of Complex II does not block electron transfer and has no effect on mitoflashes produced by Complex I substrates. Simultaneous measurement of TMRM fluorescence revealed that, in all these cases, mitoflash inhibition was accompanied by sustained $\Delta\Psi_m$ dissipation (Fig. 1, C, and F; and Fig. S3, A, B, and E), confirming the notion that electrochemical charging of mitochondria is a prerequisite for mitoflash biogenesis (Schwarzlander et al., 2011; Wei-LaPierre et al., 2013; Wang et al., 2016).

Mitoflashes supported by Complex IV substrate

To determine whether mitochondrial electrochemical charging, rather than the engagement of the entire ETC system, is

sufficient for mitoflash biogenesis, we activated part of the ETC with the Complex IV substrate ascorbate/TMPD (Fig. 2 A). In the presence of ascorbate/TMPD, Complex IV operates to transfer electrons forward from cytochrome c to oxygen molecules to form H_2O , coupled with pumping protons into the intermembrane space. Robust mitoflash activity did emerge after the establishment of $\Delta\Psi_m$ by Complex IV activity (Fig. 2, B and C; Fig. S1 B; and Video 3), indicating that partial activation of the ETC is sufficient for generating mitoflashes. This conclusion was substantiated by the fact that a Complex IV inhibitor (KCN or NaN_3) dissipated $\Delta\Psi_m$ and abolished mitoflash generation (Fig. 2, C and D; and Fig. S3 C).

To our surprise, we found that application of rotenone to inhibit Complex I dramatically enhanced mitoflash activity without altering $\Delta\Psi_m$, and using antimycin A to inhibit Complex III enhanced mitoflash activity despite decreasing $\Delta\Psi_m$ (Fig. 2, C and D; and Fig. S3 C). This stimulatory effect of Complex I and Complex III inhibitors on mitoflashes was confirmed by using piericidin A (another Complex I inhibitor) and myxothiazol (another Complex III inhibitor), both of which had little effect on $\Delta\Psi_m$ (Fig. 2, C and D; and Fig. S3 C). Likewise, the Complex II inhibitor malonate or atpenin A5 also significantly increased mitoflash activity without altering $\Delta\Psi_m$ (Fig. 2 C; and Fig. S3, C and E). These results suggest that reverse electron transfer (RET) occurs from cytochrome c to Complex III and Complex I (Nicholls and Ferguson, 2002), especially when high levels of reductive cytochrome c are generated by a Complex IV substrate (Miki et al., 1994; Sarewicz and Osyczka, 2015). Because RET is generally destructive to the establishment of $\Delta\mu_{\text{H}^+}$ across the inner mitochondrial membrane, the augmentation of mitoflashes by RET inhibition suggests that mitoflash biogenesis might participate in the homeostatic regulation of $\Delta\mu_{\text{H}^+}$. In this scenario, the mild increase of mitoflashes by Complex II inhibition with malonate or atpenin A5 suggests that Complex II also participates in RET under this experimental condition.

Mitoflashes supported by mitochondrial state III respiration

The above results were obtained in state II/IV respiration in which the ETC operation was uncoupled from ATP synthesis at Complex V. To further test the possible role of mitoflash biogenesis in the homeostatic regulation of mitochondrial $\Delta\mu_{\text{H}^+}$, we switched mitochondrial respiration from state II/IV to state III in which ADP was present to allow ETC activity to be coupled with ATP synthesis (Fig. 3 A). In light of the hypothesis that mitoflashes act to balance the increased $\Delta\mu_{\text{H}^+}$, we predicted that mitoflash activity would diminish in state III respiration when the ETC-built $\Delta\mu_{\text{H}^+}$ is used for ATP synthesis. Indeed, with all other conditions unchanged, the frequency of mitoflashes supported by Complex I, Complex II, or Complex IV substrates was decreased by 80%, 73%, or 79% in state III versus state II/IV respiration, respectively (Fig. 3, B–D). Inhibiting Complex V with oligomycin, which had little effect on mitoflashes supported by state II/IV respiration (Fig. 3, B–D), increased mitoflash frequency, restoring it to the level found in the absence of ATP synthesis (Fig. 3, B–D). These results provide strong evidence for an autoregulatory role of mitoflash biogenesis in maintaining mitochondrial electrochemical potential homeostasis.

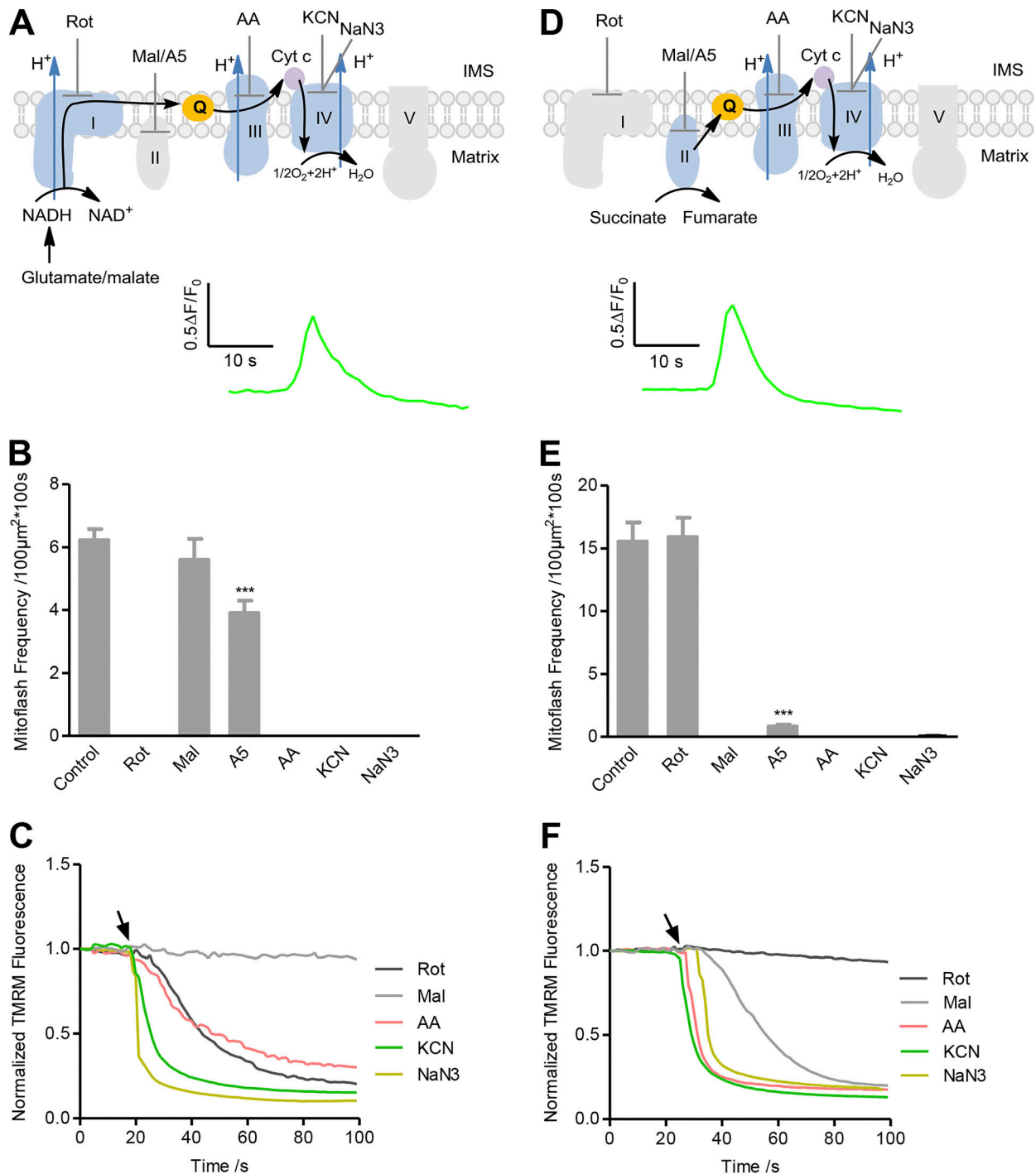


Figure 1. Full ETC-supported mitoflash biogenesis in state II/IV respiration. (A) Top: Experimental design. Complex I substrates (5 mM glutamate and 5 mM malate) without ADP were added to allow state II/IV respiration. The black arrow shows the electron transfer pathway. IMS, intermembrane space. ETC inhibitors targeting Complex I (5 μ M rotenone [Rot]), Complex II (5 mM malonate [Mal]), or 50 nM atpenin A5 [A5], Complex III (5 μ g/ml antimycin A [AA]), or Complex IV (5 mM KCN or 5 mM NaN₃) were used as designated. Bottom: Average of mitoflash traces reported with cpYFP ($n = 33$ events). **(B)** Effect of ETC inhibitors on mitoflash frequency supported by Complex I substrates. Data are mean \pm SEM, $n = 13$ –94 image series from three mice for each group. ***, $P < 0.001$ versus control group. **(C)** Averaged time courses of $\Delta\Psi_m$ measured with TMRM in response to addition of ETC inhibitors. Arrow indicates the time of inhibitor administration. $n = 3$ image series from three mice for each group. Error bars are omitted for clarity. **(D–F)** As in A–C except that a Complex II substrate (2.5 mM succinate) was used to replace Complex I substrates. $n = 61$ events for the averaged mitoflash trace in D. Data are mean \pm SEM, $n = 13$ –39 image series from three to eight mice for each group in E, ***, $P < 0.001$ versus control group. $n = 3$ image files from three mice for each trace in F. Cyt c, cytochrome c.

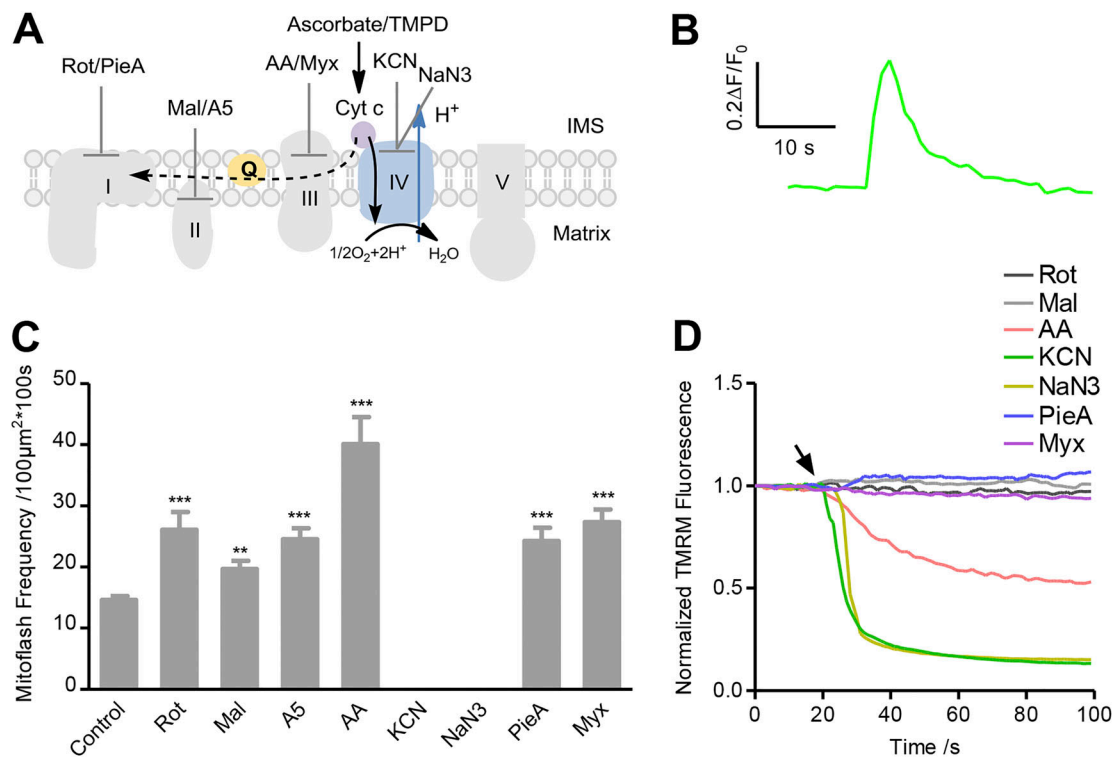


Figure 2. Partial ETC-supported mitoflash biogenesis in state II/IV respiration. (A) Experimental design. Complex IV substrates (2.5 mM ascorbate and 0.5 mM TMPD) were present without ADP. The black arrow shows the forward electron transfer pathway, and the dashed arrow shows the RET pathway. Different ETC inhibitors were also added as designated in different experimental groups (the concentrations of inhibitors were the same as in Fig. 1, and piericidin A [PieA, 1 μM] was also used for Complex I and myxothiazol [Myx, 1 μM] for Complex III). (B) Averaged trace of mitoflashes reported by cpYFP ($n = 45$ events). (C) Statistics of mitoflash frequency. Data are mean \pm SEM, $n = 14$ –134 image series from three to five mice for each group. **, $P < 0.01$; ***, $P < 0.001$ versus control group. (D) Averaged time courses of $\Delta\Psi_m$ measured with TMRM in response to addition of ETC inhibitors. Arrow indicates the time of inhibitor administration. $n = 3$ image files from three mice for each trace.

Mitoflashes supported by Complex V-mediated ATP hydrolysis

The data above show that, whether ETC is activated fully or partially, the establishment of $\Delta\mu_{H^+}$ appears to be essential for mitoflash biogenesis. In this regard, mitochondria can also develop $\Delta\mu_{H^+}$ when Complex V operates in the reverse mode, serving as an ATPase rather than an ATP synthase to pump protons outward at the cost of ATP. We therefore created an experimental condition for Complex V to operate in the reverse mode (Fig. 4 A), and determined whether mitoflashes can be generated independently of the ETC. As shown in Fig. 4 B, $\Delta\Psi_m$ was quickly established after adding ATP (3 mM) in the absence of any ETC substrates, whereas AMP-PNP, a nonhydrolysable ATP analogue, was ineffective. Importantly, robust mitoflash biogenesis occurred in the presence of ATP but not of AMP-PNP (Fig. 4, C and D; and Video 4). The average time-course showed that the unitary characteristics of these ETC-independent mitoflashes were similar to those supported by respiratory substrates except for smaller amplitude (Fig. 4 C and Fig. S2). The ATPase inhibitors oligomycin and NaN_3 abolished mitoflashes and dissipated $\Delta\Psi_m$ (Fig. 4, D and E; and Fig. S3 D), affirming that ATPase is responsible for $\Delta\Psi_m$ establishment and mitoflash biogenesis. By contrast, inhibitors of Complexes I, II, III, and IV (rotenone, atpenin A5, antimycin A, and KCN) had little effect on mitoflash activity (Fig. 4 D), indicating that the ETC does not

participate in mitoflash biogenesis under this experimental condition. But the Complex II inhibitor malonate significantly enhanced mitoflashes (Fig. 4 D). Since another Complex II inhibitor, atpenin A5, had no effect and malonate is itself a weak acid capable of generating local protons in the matrix, the enhancement of mitoflashes by malonate might be attributable to the mechanism of proton triggering of mitoflashes, which we have recently reported (Zhang et al., 2016). The antimycin A-induced slight decrease of TMRM-reported $\Delta\Psi_m$ established by ATP hydrolysis (Fig. 4 E and Fig. S3 D) might result from a nonspecific effect of antimycin A on TMRM measurement. This interpretation is consistent with the finding that antimycin A and myxothiazol had differential effects on the TMRM-reported $\Delta\Psi_m$ established by a Complex IV substrate (Fig. 2 D and Fig. S3 D). That the ATPase activity of Complex V is able to sustain mitoflash biogenesis implies that ETC per se is not obligatory in this process; rather, mitoflash activity reflects an intrinsic property of electrochemically charged mitochondria, substantiating a link between $\Delta\mu_{H^+}$ and mitoflash biogenesis.

Correlation between mitoflash amplitude and $\Delta\Psi_m$ depolarization

To demonstrate that the different signal components of mitoflashes are interlinked, we further examined the relationship between the amplitude of cpYFP-reported mitoflashes and the

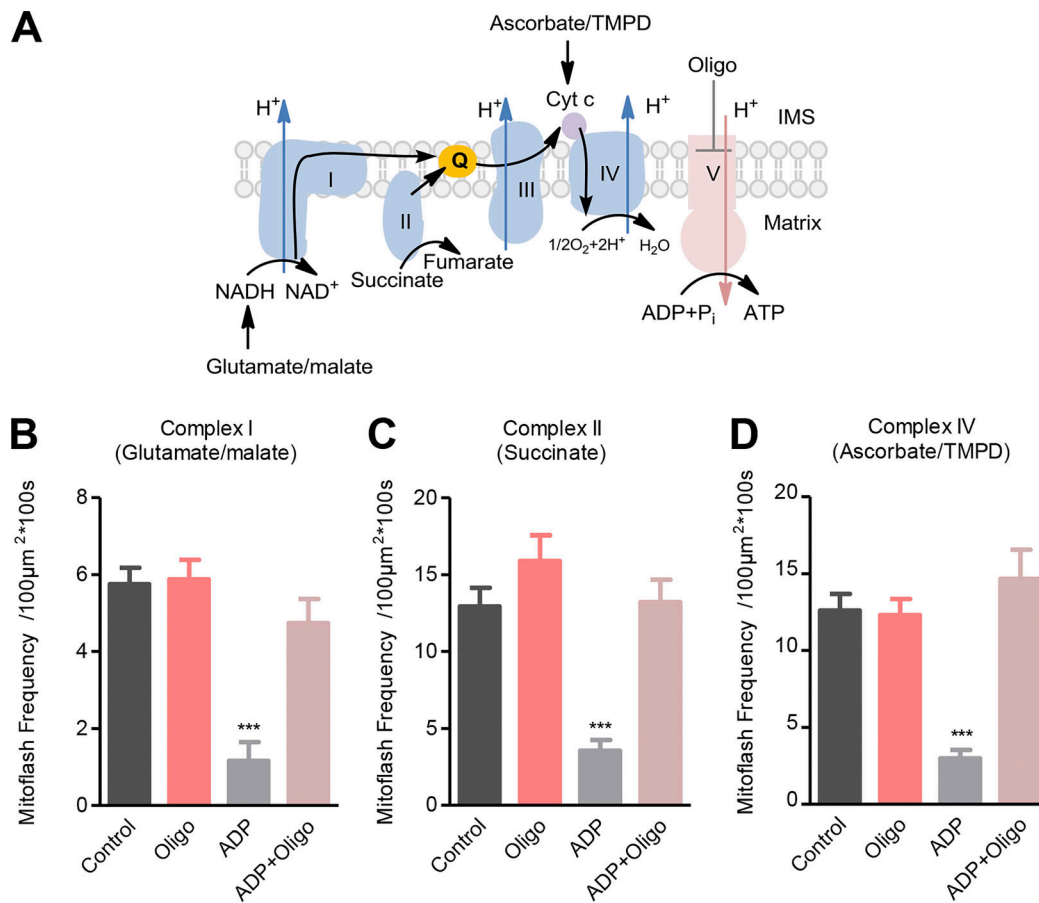


Figure 3. **Mitoflash activity mitigates in state III versus state II/IV respiration.** (A) Experimental design. In the presence of Complex I, II, or IV substrates, 200 μ M ADP was added to switch respiring mitochondria from state II/IV to state III. Oligomycin (Oligo, 5 μ M) was used to inhibit ATP synthase. The black arrow shows the electron transfer pathway. (B–D) Effects of ADP and oligomycin on mitoflash frequency supported by Complex I substrate (B), Complex II substrate (C), or Complex IV substrate (D). Data are mean \pm SEM, $n = 11$ –18 (B), 12–17 (C), and 13–16 (D) image series from three mice. ***, $P < 0.001$ ADP group versus respective control group.

companion TMRM-reported $\Delta\Psi_m$ depolarization under different experimental conditions. For this purpose, we first classified mitoflashes into two categories: type I with transient $\Delta\Psi_m$ depolarization that largely mirrored the time course of the cpYFP signal, and type II with sustained, large, and sometimes complete $\Delta\Psi_m$ depolarization that outlasted the cpYFP signal (Fig. 5 A). Both types of event coexisted in mitochondria electrochemically charged with respiratory substrates or with ATP alone. A signature feature of type II mitoflashes was that they typically displayed an overt, sustained undershoot of cpYFP fluorescence after a transient increase, potentially reflecting transient matrix acidification following the flash (Fig. 5 A and Table 1). Quantitatively, the percentages of type II mitoflashes with post-peak acidification were 85.5%, 97.4%, 48.9%, and 88.6% with Complex I, II, or IV substrates or with ATP alone, respectively. Such post-peak acidification was rarely seen in type I events (Fig. 5 A and Table 1). As we proposed previously (Hou et al., 2014), both sustained $\Delta\Psi_m$ depolarization and post-peak acidification may result from longer mitochondrial permeability transition pore (mPTP) opening at a larger subconductance. The lower proportion of type II mitoflashes in the presence of Complex IV substrate might be due to less percentage of longer

mPTP openings under this experimental condition. For type I events, linear regression analysis revealed a positive correlation between cpYFP-reported mitoflash amplitude and $\Delta\Psi_m$ depolarization in respiring mitochondria, regardless of the substrates used. In ATP-supported mitoflashes, the amplitude of cpYFP-reported mitoflashes was nearly halved (Fig. S2 A), and the correlation between mitoflash amplitude and depolarization was also weaker (Fig. 5 E). These results suggest that, in respiring mitochondria, the amplitude of mitoflash depends on the magnitude of membrane depolarization. The $\Delta\Psi_m$ dependence of proton pumping by ATPase appeared to be weaker than that of respiratory complexes.

Discussion

A unifying model for mitoflash biogenesis

Using the cell-free isolated mitochondrial system, we interrogated the biophysical and biochemical mechanisms of mitoflash biogenesis by precisely controlling the respiratory substrates and states combined with inhibition of the ETC at multiple sites, and by charging mitochondria in an ETC-independent manner. In contrast to the previous thoughts that mitoflash biogenesis

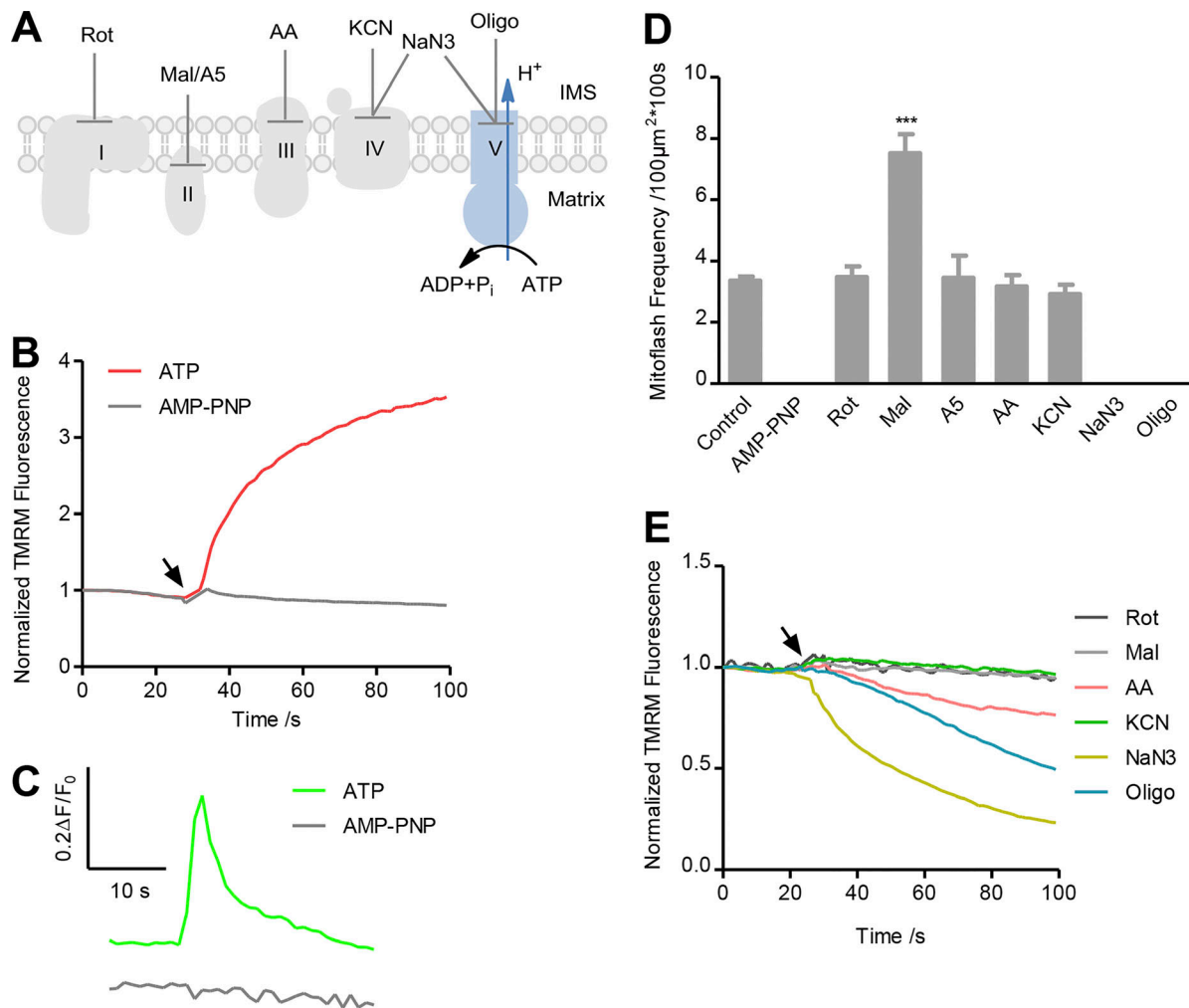


Figure 4. ATPase-supported mitoflash biogenesis. (A) Experimental design. ATP (3 mM) was present without any respiratory substrates. AMP-PNP and inhibitors were added as described to dissect the possible involvement of different ETC complexes and Complex V. (B) ATP but not AMP-PNP restored $\Delta\Psi_m$ measured with TMRM. Traces were averaged from three image series. (C) Top: Averaged trace of concurrent cpYFP-reported mitoflashes in the presence of ATP ($n = 52$ events). Bottom: No mitoflashes were recorded in the presence of AMP-PNP ($n = 22$ mitochondria). (D) Effects of ETC and ATPase inhibitors on ATPase-supported mitoflash frequency. Note also that AMP-PNP alone failed to elicit any mitoflash activity. Data are mean \pm SEM, $n = 17$ –133 image series from three mice for each group. ***, $P < 0.001$ versus control group. (E) Response of $\Delta\Psi_m$ measured with TMRM to ETC or ATPase inhibitors. Arrow indicates the time of inhibitor administration. $n = 3$ image series from three mice for each averaged trace. Error bars are omitted for clarity.

requires the integrity of ETC and ATP synthesis in the context of intact cells, we showed that the core requirement for mitoflash biogenesis lies in the establishment of mitochondrial proton electrochemical potential (Schwarzlander et al., 2011; Wei-LaPierre et al., 2013; Wang et al., 2016). Specifically, we showed that robust mitoflash activity occurred in a single mitochondrion electrochemically charged by full activation at Complex I or Complex II or, in the simplest case, partial ETC activation at Complex IV, with or without the ATP synthase activity of Complex V. More strikingly, we demonstrated that, in the presence of ATP without supplying any respiratory substrates, mitoflashes were effectively generated, in an ATPase inhibitor-sensitive (oligomycin or NaN₃), but ETC inhibitor-insensitive manner. That is, mitoflashes can be produced merely by Complex V operating in ATPase mode, independently of the ETC. Therefore, we conclude that mitoflash production is a biophysically and biochemically intrinsic

property of electrochemically energized mitochondria, providing that a trigger ignites the chemical and electrical excitation of the organelle.

This model of mitoflash biogenesis agrees well with the effects of ETC inhibitors on mitoflash activity. In general, inhibiting the forward electron flux of the ETC stops the coupled proton pumping, thus preventing the establishment of a proton electrochemical gradient across the mitochondrial inner membrane, whereas inhibiting the RET has the opposite effect. In this study, we showed that an ETC inhibitor abolished ETC-dependent mitoflashes along with depolarizing $\Delta\Psi_m$ when it acted to block forward electron transfer (i.e., at sites downstream of electron entry); however, an ETC inhibitor can also augment mitoflash frequency when it inhibits RET (see below). None of the ETC inhibitors tested, with the exception of malonate, affected the ATPase-supported mitoflashes. The effects of the ATPase inhibitor were also highly context-dependent. It

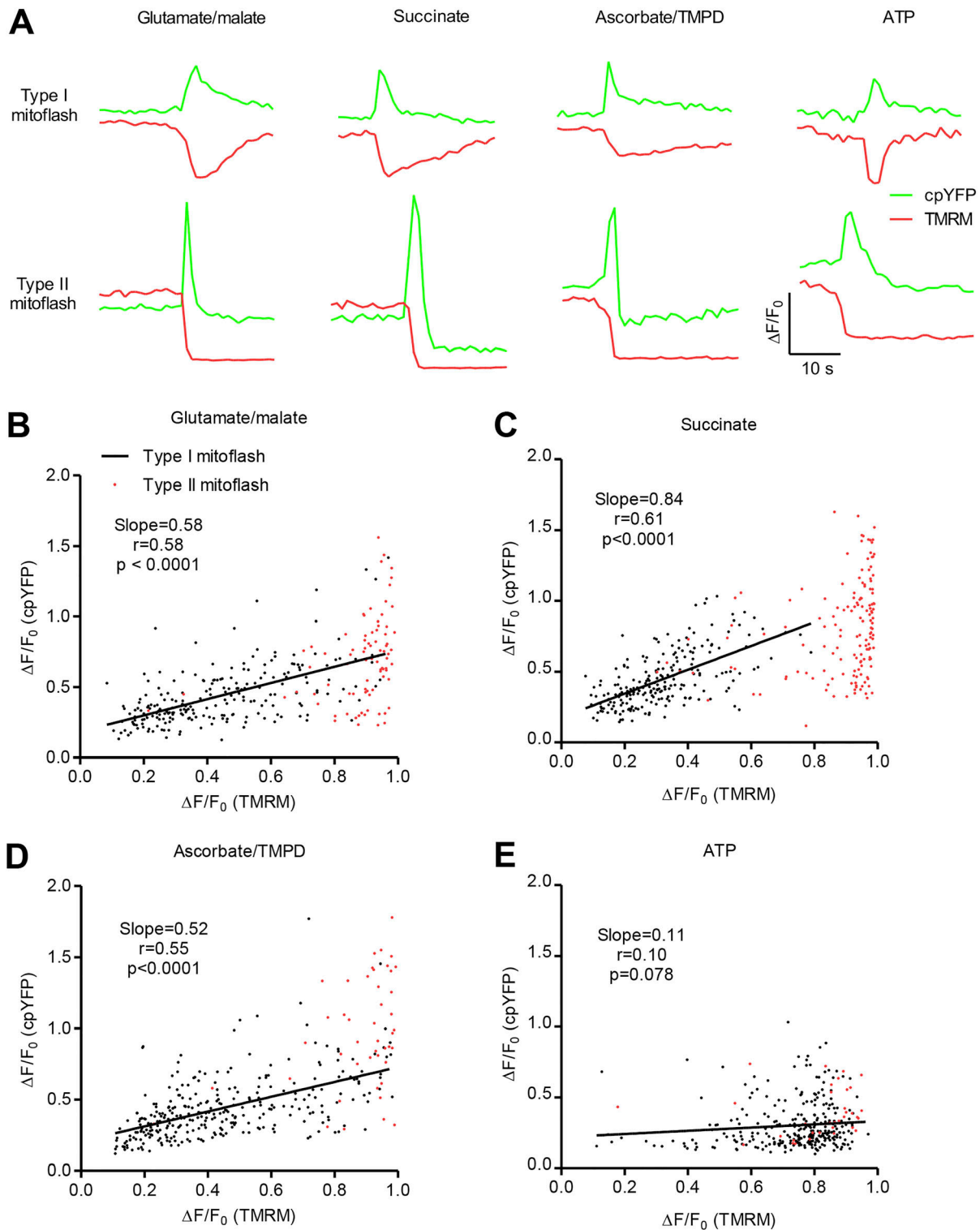


Figure 5. Correlation between mitoflash amplitude and $\Delta\Psi_m$ depolarization. (A) Representative traces of mitoflashes with transient or sustained $\Delta\Psi_m$ depolarization. Data were obtained in the presence of 5 mM glutamate/5 mM malate, 2.5 mM succinate, 2.5 mM ascorbate/0.5 mM TMPD, or 3 mM ATP. (B–E) Scatter plots for amplitude of cpYFP-reported mitoflashes and companion TMRM-reported $\Delta\Psi_m$ depolarization. Black or red dots represent events with transient or sustained $\Delta\Psi_m$ depolarization, respectively. For mitoflashes with transient $\Delta\Psi_m$ depolarization under different conditions, linear regression yielded a positive correlation between the amplitude of cpYFP-reported mitoflashes and TMRM-reported $\Delta\Psi_m$ depolarization supported by Complex I substrates ($n = 224$ events; B), Complex II substrate ($n = 222$ events; C), and Complex IV substrates ($n = 303$ events; D). Note the weak correlation between the amplitude of mitoflashes and $\Delta\Psi_m$ depolarization in ATP-supported events ($r = 0.10$, $P = 0.078$, $n = 292$ events; E). Note that sustained $\Delta\Psi_m$ depolarization was often associated with large, near-complete loss of membrane potential (red dots, $n = 83, 149, 45,$ and 35 events for data in B, C, D, and E, respectively).

Table 1. Percentages of mitoflashes with matrix acidification in different conditions

Substrates for energized mitochondria	Type I mitoflash	Type II mitoflash	χ^2	Significance
Glutamate/malate	4.9% (224)	85.5% (83)	201.1	***
Succinate	1.4% (222)	97.4% (151)	344.5	***
Ascorbate/TMPD	0% (303)	48.9% (45)	158.1	***
ATP	0.3% (292)	88.6% (35)	275.6	***

The numbers in parentheses indicate total events examined. ***, $P < 0.0001$ by χ^2 test between type I and type II mitoflash groups.

inhibited mitoflashes supported by ATPase, and was ineffective on ETC-supported events in state II/IV respiration, but enhanced mitoflashes supported by state III respiration, to a level similar to that in state II/IV respiration under otherwise the same conditions. Evidently, these diverse and sometimes opposing effects of ETC inhibitors and a Complex V inhibitor on mitoflashes can be naturally unified in the above mechanistic model of mitoflash biogenesis.

However, we and others have previously shown that mitoflash activity is repressed by all ETC inhibitors as well as a Complex V inhibitor in intact cells (Wang et al., 2008; Pouvreau, 2010; Wei et al., 2011). These once puzzling results might reflect the fact that in cells, the major electron donors are NADH for Complex I and FADH₂ for Complex II, so the entire ETC operates in such a way that all ETC inhibitors examined dissipate $\Delta\Psi_m$ and mitigate mitoflashes. Also, in intact cells, kinetic analysis of the oligomycin effect has revealed a biphasic response, an initial increase in the first 20 min before a decline of mitoflashes (Gong et al., 2015). The initial augmentation of mitoflashes is consistent with its effect on state III respiration-supported mitoflashes in isolated mitochondria, while the late inhibitory phase might reflect a secondary effect of ATP depletion in intact cells. In this regard, it has been shown that addition of ADP inhibits mitoflashes supported by Complex I or Complex II substrates in mitochondria isolated from skeletal muscle (Wei-LaPierre et al., 2013).

In addition, Gong et al. (2015) showed that rotenone inhibits mitoflashes under state III respiration in the presence of succinate and ADP in permeabilized cardiomyocytes, but our results showed that rotenone had little effect on succinate-supported mitoflashes under state II/IV respiration. The different effects of rotenone might be due to different induction mechanisms of mitoflash generation under different respiratory conditions, i.e., mitoflashes are primarily induced by ROS in the presence of succinate and ADP, and thus rotenone inhibits mitoflashes by repressing RET-mediated ROS production (Gong et al., 2015); however, in the presence of only succinate, proton leakage might be the dominant induction mechanism irrespective of the presence of RET-mediated ROS production at a relatively high level.

It has been hypothesized that transient mPTP openings serve to ignite mitoflashes (Hou et al., 2014). Given that the mPTP has multiple gating modes with different levels of subconductance and durations (Bernardi et al., 2015), mPTP openings at larger conductance with longer duration may not only trigger a mitoflash, but also induce sustained $\Delta\Psi_m$ depolarization and matrix

acidification, the latter manifesting as the undershoot after the peak of a cpYFP-reported type II mitoflash. Moreover, mitoflash amplitude was positively correlated with $\Delta\Psi_m$ depolarization in type I mitoflashes in respiring mitochondria; a similar but weaker correlation was seen among ATP-supported mitoflashes. This result might reflect the fact that proton pumps such as ETC complexes and ATPase are voltage dependent: the more the membrane is depolarized, the faster their rate of proton pumping. The sensitivity of proton pumping to $\Delta\Psi_m$ depolarization may vary among different ETC complexes and the ATPase.

Role of mitoflashes in autoregulating mitochondrial proton electrochemical potential

Our previous study showed that mitoflashes are important signaling events in regulating ATP homeostasis in the heart (Wang et al., 2017). Here, we synthesized the results from isolated mitochondria lacking cell-level metabolic regulation to provide further evidence supporting the hypothesis that the mitoflash is an intrinsic regulator of mitochondrial bioenergetics through setting the level of proton electrochemical potential, $\Delta\mu_{H^+}$. The first line of evidence comes from the observation that inhibition of RET increases mitoflashes supported by Complex IV substrate. In state II/IV respiration, proton efflux along the ETC is balanced with the basal proton leak to maintain a constant $\Delta\mu_{H^+}$ (Brand and Nicholls, 2011). In some instances, such as in the presence of Complex IV substrate, RET occurs and is associated with proton influx, which might also contribute to $\Delta\mu_{H^+}$ homeostasis (Sarewicz and Osyczka, 2015), and blocking RET tends to increase $\Delta\mu_{H^+}$, perturbing mitochondrial electrochemical homeostasis. The rise of mitoflash activity in this context can thus be interpreted as an autoregulatory mechanism to counterbalance an increasing $\Delta\mu_{H^+}$. The second line of evidence lies in the interesting result that switching from state II/IV to state III respiration markedly and reversibly decreased mitoflash frequency. This finding reinforces the logic of autoregulation of $\Delta\mu_{H^+}$, because proton influx through ATP synthase to drive ATP synthesis tends to a decrease in $\Delta\mu_{H^+}$. Together with our previous evidence that mitoflashes inhibit ATP synthesis in a cell-free mitochondrial preparation (Wang et al., 2017), we postulate that mitoflashes are a built-in autoregulator of bioenergetics at the single-mitochondrion level. More specifically, by sensing and responding to perturbations of mitochondrial $\Delta\mu_{H^+}$, mitoflash activity waxes and wanes to maintain and safeguard $\Delta\mu_{H^+}$ homeostasis in a manner akin to the safety valve on a steam engine.

It should be noted that, by exploiting its multiplex signals, the mitoflash can be multifunctional depending on the cellular and subcellular contexts. Besides its role in mitochondrial bioenergetics, mitoflash biogenesis also affords a mechanism to produce intense, local, and transient ROS signals under physiological conditions. In this regard, we have recently reported that mitoflashes are essential signaling events that participate in stabilizing long-term synaptic plasticity in neurons (Fu et al., 2017).

In summary, mitoflash biogenesis is an intrinsic activity of electrochemically charged mitochondria, requiring neither intact oxidative phosphorylation nor ETC activity in isolated mitochondria under experimental conditions. Mitoflash activity appears to respond to and counteract perturbations that alter the electrochemical charging of mitochondria. Based on the cell and organelle logic of mitoflash biogenesis, we propose that, in addition to other functions, mitoflashes serve as a homeostatic auto-regulator of mitochondrial proton electrochemical potential. As such, targeting mitoflash biogenesis might provide a new means of intervening energy metabolism as well as mitochondrial signaling in health and disease.

Acknowledgments

We thank Dr. Paolo Bernardi for critical comments and Dr. Tingting Hou, Mr. Rongkang Yin, and Mr. Peng Yu for technical assistance.

This work was supported by the National Key Basic Research Program of China (2016YFA0500403, 2017YFA0504002, and 2013CB531200) and the National Science Foundation of China (31470811, 31670039, and 31821091).

The authors declare no competing financial interests.

Author contributions: H. Cheng and X. Wang conceived and supervised the study. G. Feng performed experiments and analyzed data with help from Z. Huang and T. Cheng. B. Liu contributed to the theoretical interpretation of the data. J. Li developed imaging processing algorithms and software. X. Wang and H. Cheng wrote the paper with input from all authors. All participated in data interpretation.

Eduardo Ríos served as editor.

Submitted: 10 July 2018

Revised: 29 November 2018

Accepted: 19 February 2019

References

- Bernardi, P., A. Rasola, M. Forte, and G. Lippe. 2015. The mitochondrial permeability transition pore: Channel formation by F-ATP synthase, integration in signal transduction, and role in pathophysiology. *Physiol. Rev.* 95:1111–1155. <https://doi.org/10.1152/physrev.00001.2015>
- Brand, M.D., and D.G. Nicholls. 2011. Assessing mitochondrial dysfunction in cells. *Biochem. J.* 435:297–312. <https://doi.org/10.1042/BJ20110162>
- Breckwoldt, M.O., F.M. Pfister, P.M. Bradley, P. Marinković, P.R. Williams, M.S. Brill, B. Plomer, A. Schmalz, D.K. St Clair, R. Naumann, et al. 2014. Multiparametric optical analysis of mitochondrial redox signals during neuronal physiology and pathology in vivo. *Nat. Med.* 20:555–560. <https://doi.org/10.1038/nm.3520>
- Fang, H., M. Chen, Y. Ding, W. Shang, J. Xu, X. Zhang, W. Zhang, K. Li, Y. Xiao, F. Gao, et al. 2011. Imaging superoxide flash and metabolism-coupled mitochondrial permeability transition in living animals. *Cell Res.* 21:1295–1304. <https://doi.org/10.1038/cr.2011.81>
- Feng, G., B. Liu, T. Hou, X. Wang, and H. Cheng. 2017. Mitochondrial Flashes: Elemental Signaling Events in Eukaryotic Cells. *Handb. Exp. Pharmacol.* 240:403–422. https://doi.org/10.1007/164_2016_129
- Fu, Z.X., X. Tan, H. Fang, P.M. Lau, X. Wang, H. Cheng, and G.Q. Bi. 2017. Dendritic mitoflash as a putative signal for stabilizing long-term synaptic plasticity. *Nat. Commun.* 8:31. <https://doi.org/10.1038/s41467-017-00043-3>
- Gong, G., X. Liu, H. Zhang, S.S. Sheu, and W. Wang. 2015. Mitochondrial flash as a novel biomarker of mitochondrial respiration in the heart. *Am. J. Physiol. Heart Circ. Physiol.* 309:H1166–H1177. <https://doi.org/10.1152/ajpheart.00462.2015>
- Hou, T., X. Zhang, J. Xu, C. Jian, Z. Huang, T. Ye, K. Hu, M. Zheng, F. Gao, X. Wang, and H. Cheng. 2013. Synergistic triggering of superoxide flashes by mitochondrial Ca²⁺ uniport and basal reactive oxygen species elevation. *J. Biol. Chem.* 288:4602–4612. <https://doi.org/10.1074/jbc.M112.398297>
- Hou, T., X. Wang, Q. Ma, and H. Cheng. 2014. Mitochondrial flashes: new insights into mitochondrial ROS signalling and beyond. *J. Physiol.* 592:3703–3713. <https://doi.org/10.1113/jphysiol.2014.275735>
- Jian, C., T. Hou, R. Yin, H. Cheng, and X. Wang. 2014. Regulation of superoxide flashes by transient and steady mitochondrial calcium elevations. *Sci. China Life Sci.* 57:495–501. <https://doi.org/10.1007/s11427-014-4628-z>
- Jian, C., F. Xu, T. Hou, T. Sun, J. Li, H. Cheng, and X. Wang. 2017. Deficiency of PHB complex impairs respiratory supercomplex formation and activates mitochondrial flashes. *J. Cell Sci.* 130:2620–2630. <https://doi.org/10.1242/jcs.198523>
- Li, K., W. Zhang, H. Fang, W. Xie, J. Liu, M. Zheng, X. Wang, W. Wang, W. Tan, and H. Cheng. 2012. Superoxide flashes reveal novel properties of mitochondrial reactive oxygen species excitability in cardiomyocytes. *Biophys. J.* 102:1011–1021. <https://doi.org/10.1016/j.bpj.2012.01.044>
- Mailloux, R.J. 2015. Teaching the fundamentals of electron transfer reactions in mitochondria and the production and detection of reactive oxygen species. *Redox Biol.* 4:381–398. <https://doi.org/10.1016/j.redox.2015.02.001>
- Miki, T., M. Miki, and Y. Orii. 1994. Membrane potential-linked reversed electron transfer in the beef heart cytochrome b_c1 complex reconstituted into potassium-loaded phospholipid vesicles. *J. Biol. Chem.* 269:1827–1833.
- Mitchell, P. 1966. Chemiosmotic coupling in oxidative and photosynthetic phosphorylation. *Biol. Rev. Camb. Philos. Soc.* 41:445–502. <https://doi.org/10.1111/j.1469-185X.1966.tb01501.x>
- Miyadera, H., K. Shiomi, H. Ui, Y. Yamaguchi, R. Masuma, H. Tomoda, H. Miyoshi, A. Osanai, K. Kita, and S. Omura. 2003. Atpenins, potent and specific inhibitors of mitochondrial complex II (succinate-ubiquinone oxidoreductase). *Proc. Natl. Acad. Sci. USA.* 100:473–477. <https://doi.org/10.1073/pnas.0237315100>
- Nicholls, D.G., and S.L. Ferguson. 2002. *Bioenergetics*. Academic Press, London, San Diego.
- Pouvreau, S. 2010. Superoxide flashes in mouse skeletal muscle are produced by discrete arrays of active mitochondria operating coherently. *PLoS One.* 5:e13035. <https://doi.org/10.1371/journal.pone.0013035>
- Sarewicz, M., and A. Osyczka. 2015. Electronic connection between the quinone and cytochrome C redox pools and its role in regulation of mitochondrial electron transport and redox signaling. *Physiol. Rev.* 95:219–243. <https://doi.org/10.1152/physrev.00006.2014>
- Schwarzländer, M., D.C. Logan, M.D. Fricker, and L.J. Sweetlove. 2011. The circularly permuted yellow fluorescent protein cpYFP that has been used as a superoxide probe is highly responsive to pH but not superoxide in mitochondria: implications for the existence of superoxide ‘flashes’. *Biochem. J.* 437:381–387. <https://doi.org/10.1042/BJ20110883>
- Shadel, G.S., and T.L. Horvath. 2015. Mitochondrial ROS signaling in organismal homeostasis. *Cell.* 163:560–569. <https://doi.org/10.1016/j.cell.2015.10.001>
- Shen, E.Z., C.Q. Song, Y. Lin, W.H. Zhang, P.F. Su, W.Y. Liu, P. Zhang, J. Xu, N. Lin, C. Zhan, et al. 2014. Mitoflash frequency in early adulthood predicts lifespan in *Caenorhabditis elegans*. *Nature.* 508:128–132. <https://doi.org/10.1038/nature13012>
- Wang, W., H. Fang, L. Groom, A. Cheng, W. Zhang, J. Liu, X. Wang, K. Li, P. Han, M. Zheng, et al. 2008. Superoxide flashes in single mitochondria. *Cell.* 134:279–290. <https://doi.org/10.1016/j.cell.2008.06.017>
- Wang, X., X. Zhang, Z. Huang, D. Wu, B. Liu, R. Zhang, R. Yin, T. Hou, C. Jian, J. Xu, et al. 2016. Protons Trigger Mitochondrial Flashes. *Biophys. J.* 111:386–394. <https://doi.org/10.1016/j.bpj.2016.05.052>

- Wang, X., X. Zhang, D. Wu, Z. Huang, T. Hou, C. Jian, P. Yu, F. Lu, R. Zhang, T. Sun, et al. 2017. Mitochondrial flashes regulate ATP homeostasis in the heart. *eLife*. 6:e23908. <https://doi.org/10.7554/eLife.23908>
- Wei, L., G. Salahura, S. Boncompagni, K.A. Kasischke, F. Protasi, S.S. Sheu, and R.T. Dirksen. 2011. Mitochondrial superoxide flashes: metabolic biomarkers of skeletal muscle activity and disease. *FASEB J*. 25: 3068–3078. <https://doi.org/10.1096/fj.11-187252>
- Wei-LaPierre, L., G. Gong, B.J. Gerstner, S. Ducreux, D.I. Yule, S. Pouvreau, X. Wang, S.S. Sheu, H. Cheng, R.T. Dirksen, and W. Wang. 2013. Respective contribution of mitochondrial superoxide and pH to mitochondria-targeted circularly permuted yellow fluorescent protein (mt-cpYFP) flash activity. *J. Biol. Chem.* 288:10567–10577. <https://doi.org/10.1074/jbc.M113.455709>
- Zhang, J., X. Wang, V. Vikash, Q. Ye, D. Wu, Y. Liu, and W. Dong. 2016. ROS and ROS-Mediated Cellular Signaling. *Oxid. Med. Cell. Longev.* 2016: 4350965. <https://doi.org/10.1155/2016/4350965>
- Zhang, M., T. Sun, C. Jian, L. Lei, P. Han, Q. Lv, R. Yang, X. Zhou, J. Xu, Y. Hu, et al. 2015. Remodeling of Mitochondrial Flashes in Muscular Development and Dystrophy in Zebrafish. *PLoS One*. 10:e0132567. <https://doi.org/10.1371/journal.pone.0132567>
- Zhang, W., K. Li, X. Zhu, D. Wu, W. Shang, X. Yuan, Z. Huang, M. Zheng, X. Wang, D. Yang, et al. 2014. Subsarcolemmal mitochondrial flashes induced by hypochlorite stimulation in cardiac myocytes. *Free Radic. Res.* 48:1085–1094. <https://doi.org/10.3109/10715762.2014.932114>
- Zhang, X., Z. Huang, T. Hou, J. Xu, Y. Wang, W. Shang, T. Ye, H. Cheng, F. Gao, and X. Wang. 2013. Superoxide constitutes a major signal of mitochondrial superoxide flash. *Life Sci.* 93:178–186. <https://doi.org/10.1016/j.lfs.2013.06.012>